Energy Conversion and Management 366 (2026) 121885

Contents lists available at ScienceDirect

Energy Conversion and Management

journal homepage: www.elsevier.com/locate/enconman

Pressure-regulated pool boiling for lithium-ion batteries based on a thermo-lifetime-economic coupling framework

Xiang Wang, Liang Li *, Savvas A. Tassou

College of Engineering, Design and Physical Sciences, Brunel University of London, Uxbridge UB8 3PH, UK

ARTICLE INFO

Keywords:
Pool boiling
Pressure-controlled
Lithium-ion battery module
Thermal management
Energy efficiency

ABSTRACT

Pool boiling cooling offers strong potential for lithium-ion battery thermal management due to its high-efficiency phase-change heat transfer. However, most existing studies are limited to atmospheric pressure, and the coupled effects of pressure on thermal behaviour, battery lifetime, and economic performance remain unclear. In this study, a thermo-lifetime-economic coupling model is developed and experimentally validated through pressure-controlled pool boiling cooling of a battery module over a pressure range of 20–100 kPa. The results show that pool boiling significantly outperforms natural air-cooling, reducing the maximum temperature from 88.8 °C to 45.6 °C (48.6%) and the temperature difference from 9.3 °C to 3.1 °C (66.7%) at 2.5C. Further pressure reduction enhances thermal performance by lowering the saturation temperature and promoting earlier nucleate boiling. When the pressure decreases from 100 kPa to 20 kPa, the maximum temperature and temperature difference are further reduced by 26.3% and 38.7%, respectively, leading to a lifetime improvement of up to 65.1%. However, this improvement is accompanied by a substantial increase in auxiliary power consumption, which rises by more than 14.6 times, resulting in a strong thermo-economic trade-off with diminishing returns at low pressures. Furthermore, system scale critically affects economic feasibility. Pressure reduction increases cost at small scales but becomes favourable beyond a critical scale due to the growing contribution of lifetime-related cost. These results show that pressure regulation can improve pool boiling battery cooling, but the operating pressure should balance thermal performance, lifetime, and energy consumption.

1. Introduction

Under high C-rate charge and discharge conditions, effective thermal management of lithium-ion battery modules is critical to ensuring operational safety, maintaining electrochemical performance, and extending service life [1,2]. Such operating conditions are commonly encountered in heavy-duty electric trucks, construction machinery, and track-oriented vehicles. In these systems, battery modules often operate under sustained high load conditions, which can readily lead to heat accumulation [3,4]. If the generated heat is not removed in a timely and effective manner, batteries may experience excessively high operating temperatures and pronounced temperature non-uniformity. Elevated temperatures and the associated thermal gradients not only accelerate battery ageing and degrade electrochemical performance, but also substantially increase safety risks [5]. Under sustained high-load conditions, conventional single-phase cooling strategies may approach their thermal management limits. Consequently, advanced battery thermal management systems capable of achieving efficient heat dissipation under high heat flux conditions while maintaining good temperature uniformity have become a major focus of current research.

In recent years, immersion cooling technologies based on phase-change heat transfer have been widely regarded as a highly promising high-performance solution for battery thermal management [6,7]. Compared with conventional single-phase cooling approaches such as natural convection and forced convection, two-phase cooling can exploit the latent heat associated with phase change, thereby achieving significantly higher heat transfer coefficients and reduced temperature differences. Pool boiling cooling is characterised by low wall superheat, high heat transfer efficiency, and great temperature uniformity [8,9]. It is well suited to the thermal management of battery modules operating under high heat load conditions. Existing studies have demonstrated that pool boiling can effectively suppress peak battery temperatures and offers clear advantages over single-phase cooling strategies in improving temperature uniformity [10–12].

Despite the demonstrated advantages of pool boiling cooling in battery thermal management, there remains considerable scope for

* Corresponding author.
E-mail address: Liang.Li@brunel.ac.uk (L. Li).

https://doi.org/10.1016/j.enconman.2026.121885
Received 17 April 2026; Received in revised form 25 June 2026; Accepted 6 July 2026
Available online 11 July 2026

further improvement. The enhancement of pool boiling heat transfer performance has been mainly investigated through modifications of boiling surface characteristics, structural design, and external disturbances [13,14]. In addition, structural enhancement strategies developed for single-phase battery thermal management systems have also demonstrated considerable potential for improving heat transfer performance. Qi et al. [15] reported that liquid-cooling plate channels embedded with non-uniform spiral fin structures can significantly enhance heat transfer and improve temperature uniformity. Lyu [16] demonstrated that increasing the surface roughness of battery can promote bubble nucleation and detachment, thereby reducing the temperature difference during charge and discharge to approximately 2.7–2.9 °C. Williams [17] enhanced bubble interactions and fluid disturbances between adjacent cells by reducing the battery spacing. It leads to a slight reduction in battery temperature and an improvement in thermal uniformity within the battery module. In addition, Kim [18] found that promoting bubble detachment and liquid renewal through the introduction of structural motion can effectively enhance the pool boiling heat transfer. These approaches not only increase system complexity and manufacturing cost but also limit their general applicability and engineering feasibility in practical battery systems. By contrast, regulating the pool boiling from the system operating conditions remains a relatively less explored yet promising approach for heat transfer enhancement. From the heat transfer mechanism perspective, system pressure plays a crucial role in governing the pool boiling [19]. Reducing the system pressure markedly lowers the saturation temperature of the working fluid, enabling boiling to be initiated at lower wall temperatures. It can promote the earlier onset of nucleate boiling and enhances pool boiling heat transfer. Recent studies have further highlighted the important role of pressure in pool boiling heat transfer. Kim et al. [20] comprehensively reviewed recent advances in pool boiling under different pressure and subcooling conditions, emphasizing the significant influence of operating pressure on bubble dynamics and heat transfer performance. Yu et al. [21] experimentally demonstrated that liquid static pressure strongly affects the critical heat flux characteristics of dielectric fluid Novec 7100 under low-pressure boiling conditions. He et al. [22] investigated vapor bubble growth behaviour over a wide pressure range and revealed the strong dependence of bubble dynamics on system pressure. These studies have primarily focused on fundamental boiling mechanisms and heat transfer characteristics. However, the application of pressure regulation as an active thermal management strategy for lithium-ion battery systems remains largely unexplored. In particular, a systematic understanding of how pressure affects the overall thermal response and temperature uniformity of battery modules is still lacking. As summarised in Table 1, existing studies have mainly focused on thermal performance enhancement through pool boiling or immersion cooling technologies.

In addition to thermal performance, the pool boiling cooling systems is closely associated with battery degradation and system-level energy consumption [30,31]. Lower operating temperatures can significantly extend battery lifetime, while pressure regulation introduces additional auxiliary energy demand [32,33]. Therefore, pressure control may simultaneously influence thermal behaviour, lifetime performance, and economic cost. However, most existing studies focus primarily on heat transfer enhancement, with limited attention paid to the coupled thermo–lifetime–economic effects and their implications for system design. In particular, the role of system scale in determining economic feasibility remains largely unexplored. In response to these gaps, this study presents a systematic investigation of pressure-regulated pool boiling cooling for lithium-ion battery modules, with particular emphasis on the coupled effects of pressure on thermal performance, battery lifetime, and economic feasibility. Fig. 1 illustrates the overall workflow of the proposed thermo–lifetime–economic framework. A pressure-controlled pool boiling cooling system was developed and experimentally evaluated over a wide pressure range of 20–100 kPa. The thermal responses of the battery module under different operating pressures were systematically characterised, and the underlying pressure-dependent boiling heat transfer mechanisms were analysed. Furthermore, a thermo–lifetime–economic coupling framework was established to quantify the trade-offs among cooling enhancement, lifetime extension, and auxiliary energy consumption. The influence of system scale on the

Table 1
Comparison of representative immersion cooling studies for lithium-ion battery thermal management.

Ref.	Battery	Coolant	Key findings	Limitations
Van Gils et al. [23] (2014)	Li-ion battery	Boiling coolant	Demonstrated the feasibility of boiling heat transfer for battery thermal management and achieved effective temperature control.	Focused on single-cell thermal performance; no module-level assessment.
Al-Zareer et al. [24] (2017)	High-power Li-ion battery pack	Dielectric fluid	Proposed a boiling-based BTMS capable of maintaining acceptable battery temperatures under high-power operation.	Limited analysis of boiling control parameters and economic performance.
Jithin and Rajesh [25] (2022)	Li-ion battery module	Various dielectric fluids	Compared dielectric coolants and demonstrated the importance of coolant properties on immersion cooling performance.	Investigated single-phase immersion cooling only.
Wang et al. [12] (2023)	Li-ion battery module	Dielectric fluid	Experimentally demonstrated the effectiveness of two-phase immersion cooling in reducing battery temperature.	Focused primarily on thermal performance.
Li et al. [26] (2023)	18,650 battery pack	Fluorinated liquid	Improved temperature uniformity and suppressed peak battery temperature.	Atmospheric-pressure operation only.
Williams et al. [17] (2024)	Four-cell battery module	Dielectric fluid	Experimentally validated liquid immersion cooling and enhanced module thermal uniformity.	No pressure regulation considered.
Li et al. [27] (2024)	4680 battery	Dielectric fluid	Demonstrated effective thermal management of large-format batteries using two-phase immersion cooling.	Thermal performance only; no lifetime analysis.
Lyu et al. [16] (2025)	Li-ion battery	Dielectric fluid	Surface microtopography promoted bubble nucleation and enhanced boiling heat transfer.	Requires surface modification and manufacturing complexity.
Jiang et al. [28] (2025)	Li-ion battery	Dielectric fluid	Proposed immersed evaporation and cell inversion strategy to further improve cooling efficiency.	Increased system complexity.
Wang et al. [29] (2025)	Li-ion battery module	Dielectric fluid	Investigated thermal behaviour under sloshing excitation and revealed dynamic cooling characteristics.	Did not consider pressure-controlled boiling.

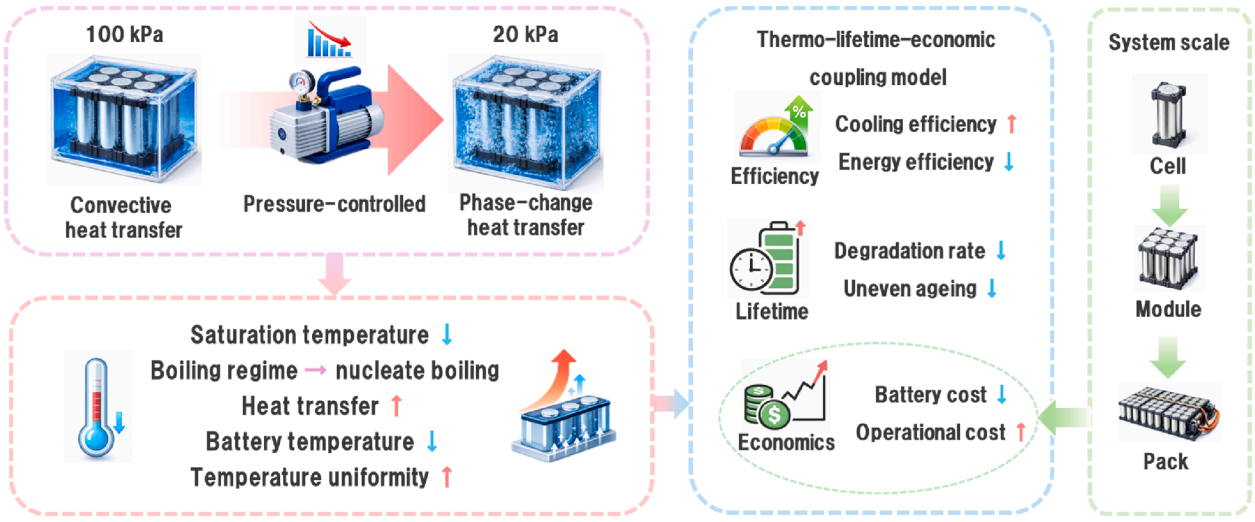

Fig.1. Thermo–lifetime–economic framework for pressure-controlled boiling battery cooling.

economic performance of pressure-regulated cooling was also investigated.

Compared with previous studies that primarily focused on thermal performance under atmospheric conditions, this work extends the evaluation of pool boiling battery thermal management beyond heat transfer enhancement by incorporating battery degradation and economic performance into a unified framework. The main contributions of this study are summarised as follows:

(1) A pressure-regulated pool boiling battery thermal management platform was developed and experimentally investigated over a pressure range of 20–100 kPa.

(2) The effects of pressure on battery temperature evolution, temperature uniformity, and boiling heat transfer behaviour were systematically quantified.

(3) A thermo–lifetime–economic coupling framework was established to evaluate the combined impacts of pressure regulation on thermal performance, battery degradation, and operating cost.

(4) The trade-offs between cooling enhancement and auxiliary energy consumption were revealed, and the influence of system scale on the economic viability of pressure-regulated cooling was quantitatively assessed.

2. Experimental setup and methodology

2.1. Battery module and experimental system

In this study, lithium-ion batteries (INR21700-50G) manufactured by Samsung were selected. Its key specifications are listed in Table 2 [34].

The experimental battery module consisted of seven lithium-ion cells connected in series in a clover-shaped arrangement, as illustrated in Fig. 2. This configuration is representative of the typical characteristics of compact battery modules [35]. Meanwhile, twenty-one K-type

Table 2
Key parameters of the lithium-ion battery.

Parameter	Value
Battery model	Samsung INR21700-50G
Battery format	21,700 cylindrical battery
Battery chemistry	NCA ($LiNiCoAlO_2$)
Nominal capacity (mAh)	4900
Charge cut-off voltage (V)	4.20
Discharge cut-off voltage (V)	2.50
Maximum continuous discharge current (mA)	9800

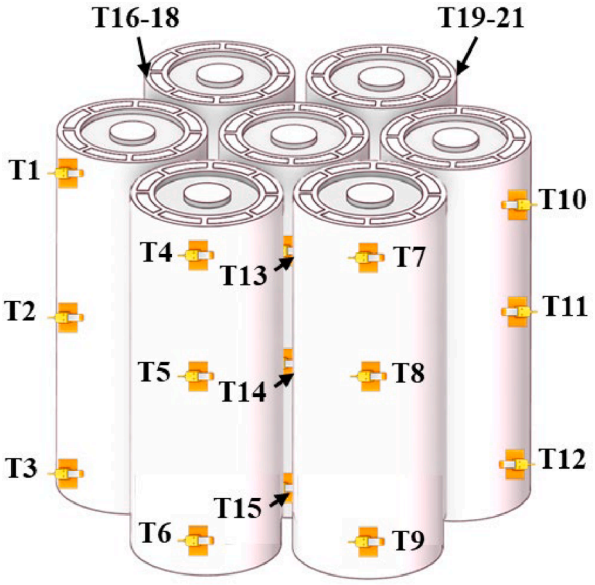

Fig. 2. Schematic of the battery module.

thermocouples were attached to the cell surfaces using thermally conductive adhesive tape to monitor the temperature distribution during the experiments.

The heat generation behaviour of the battery during discharge was characterised through near-adiabatic temperature rise experiments on a single battery. The battery and were placed inside a temperature-controlled chamber (DHP-9022, RENUO Instrument Equipment Co., Ltd., China) to maintain a constant temperature throughout the experiments. Constant-current discharge was performed using a TEC-80K programmable DC electronic load (Shunda Electronics Co., Ltd., China). Thermal insulation materials were applied around the battery to minimise heat exchange with the surrounding environment. The insulation materials are polyurethane foam with a total thickness of approximately 30 mm and a thermal conductivity of about 0.03 $W{\cdot}m^{-1}{\cdot}K^{-1}$. Three K-type thermocouples (Omega Engineering Inc., USA) were attached to the battery surface to monitor temperature variations in real time, and the temperature-time data were recorded using a data acquisition system. The experimental setup is shown in Fig. 3.

The battery module was fully immersed in a sealed immersion

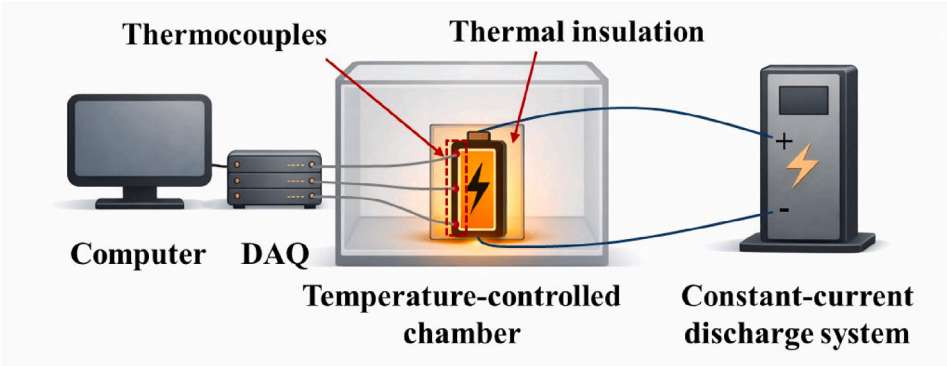

Fig. 3. Schematic of the quasi-adiabatic temperature rise setup.

cooling chamber filled with a dielectric coolant. KEY-116 (Zhongke Micro New Materials Co., Ltd., China). was selected as the working fluid because its thermophysical and dielectric properties are well suited for battery immersion cooling. Compared with many conventional fluorinated dielectric fluids, KEY-116 possesses a moderate boiling point (65 °C), low viscosity, high electrical insulation capability, good chemical stability, and non-flammability, which facilitate efficient boiling heat transfer while ensuring electrical safety [36]. The thermophysical properties are summarised in Table 3.

The pool boiling cooling system integrates pressure, liquid level, and temperature regulation functions. It includes a chamber, a pressure regulation system, a temperature regulation system, a liquid replenishment and recovery system, and a data acquisition and control system. The chamber was lined with thermal insulation and used to accommodate the battery module and coolant. It provided a sealed experimental environment to minimise heat exchange with the surroundings and maintain system pressure stability. Consequently, the heat loss to the ambient environment was expected to be relatively small compared with the battery heat generation, and a near-adiabatic assumption was adopted in the present analysis. The pressure regulation system was employed to adjust and maintain the internal pressure of the chamber. Precise pressure control was achieved using a vacuum pump (Feiyue Vacuum Pump Co., Ltd., China), a pressure sensor (VIDAS Co., Ltd., China), and a pressure buffer tank. The operating pressure range was 20–100 kPa. The temperature regulation system was implemented using heating elements and temperature sensors to control the initial temperature of the coolant. It was also used to ensure temperature uniformity, thereby maintaining consistent experimental conditions under different operating cases. To enable visual observation of the boiling process, a high-speed imaging system (Revealer Co., Ltd., China) was installed alongside the boiling chamber to capture bubble dynamics under different operating conditions. A schematic diagram and photograph of the entire pool boiling battery module cooling test rig are presented in Fig. 4.

Table 3
Physical and thermophysical properties of KEY-116.

Property	Value	Property	Value
Boiling point	65 ℃	Thermal conductivity	0.065 W/mK
Dynamic viscosity	0.524 cp (25℃)	Dielectric constant	1.88
Vapor pressure	0.404 bar (25℃)	Density	1.65 g/cc
Specific heat capacity	1.013 kJ/kg℃	Latent heat of vaporization	88.0 kJ/kg
Thermal expansion coefficient	0.0011 cm^3/cm^3℃	Surface tension	14 dyne/cm

2.2. Experimental conditions and test procedure

Temperature rise experiments were conducted on a single battery under near-adiabatic conditions to characterize the temperature evolution during discharge. Prior to testing, the battery was allowed to rest for 3 h at an ambient temperature of approximately 25 °C to ensure thermal equilibrium between the battery and the surrounding environment. During the experiments, constant-current discharge tests were performed at discharge rates ranging from 1.0 C to 2.5 C. Throughout the discharge process, the battery surface temperature was continuously recorded using a data acquisition system to obtain temperature–time data under different operating conditions.

For the pool boiling cooling experiments, the battery module was first charged to the cut-off voltage and subsequently allowed to rest under ambient conditions for 3 h to eliminate the influence of previous charge–discharge history on the initial thermal state. Subsequently, the boiling chamber was filled with approximately 4.3 L of KEY-116 dielectric coolant. A liquid-level stabilisation system was continuously operated to maintain a constant coolant level throughout the experiment. The coolant level was maintained approximately 10 mm above the top surface of the battery module to ensure complete immersion under all operating conditions. To minimise coolant loss during boiling, a condenser and condensate recovery system were employed. The generated vapour was condensed and returned to the boiling chamber, thereby maintaining a stable coolant inventory throughout the experiments.

Following this, the temperature regulation system was activated to adjust and maintain the coolant at the preset initial temperature. During the temperature stabilisation stage, the coolant temperature fluctuation was maintained within ±0.5 °C of the target value. Once the coolant temperature reached the target value, the pressure regulation system was activated to control the chamber pressure within the desired range of 20–100 kPa. The pressure control system consisted of a vacuum pump, a pressure transducer, an electronic control valve, and a pressure buffer tank. To improve pressure stability during pool boiling operation, the pressure buffer tank was installed between the boiling chamber and the vacuum pump. By increasing the effective system volume, the buffer tank effectively damped transient pressure fluctuations caused by rapid vapour generation, condensate reflux, and intermittent vacuum pump operation, thereby reducing the direct influence of vacuum pumping on the chamber pressure. During the experiments, the chamber pressure was continuously monitored and automatically regulated through a closed-loop control strategy. The pressure fluctuation was maintained within ±0.8 kPa of the target pressure throughout the experiments.

Prior to each discharge test, the system was maintained under the prescribed temperature and pressure conditions for approximately 30 min to ensure a stable and uniform initial state of both the battery module and the coolant. After completing the above preparatory procedures, the discharge experiments were initiated, with the battery

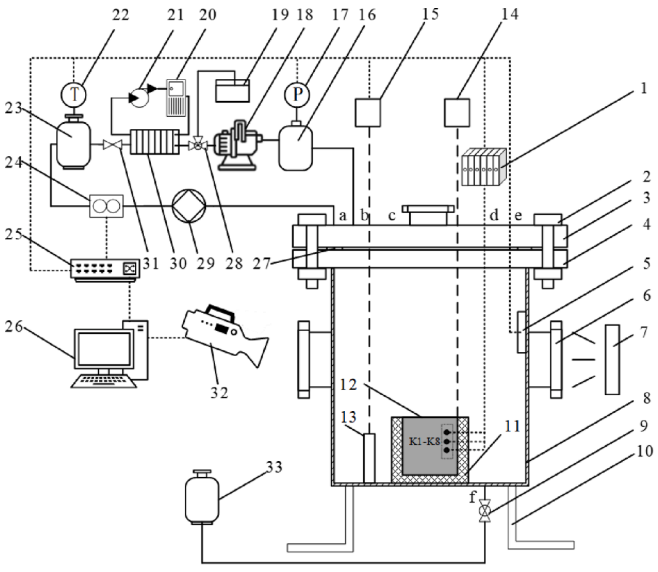

1 Temperature transmitter
2 Bolt
3 Upper flange cover plate
4 Lower flange cover plate
5 Capacitive liquid level sensor
6 Sight window
7 Flicker-free light source
8 Boiling chamber
9 Drain valve
10 Support frame
11 Battery module housing
12 Battery module
13 Auxiliary heater
14 Constant-current discharge system
15 Adjustable DC power supply
16 Vacuum buffer tank
17 Pressure sensor
18 Vacuum pump
19 Water tank
20 Constant-temperature bath
21 Circulating water pump
22 Electronic liquid thermometer
23 Condensate storage tank
24 Flow meter
25 Data acquisition card
26 Computer
27 Sealing ring
28 Three-way valve
29 Transfer pump
30 Plate condenser
31 Temperature control valve
32 High-speed camera
33 Coolant recovery tank

K1–K8 Type-K thermocouples

a Condensate return port
b Vacuum port
c Electrical wiring interface
d Temperature sensor signal interface
e Liquid level sensor signal interface
f Drain outlet

(a) Schematic diagram of pool boiling battery module cooling test rig

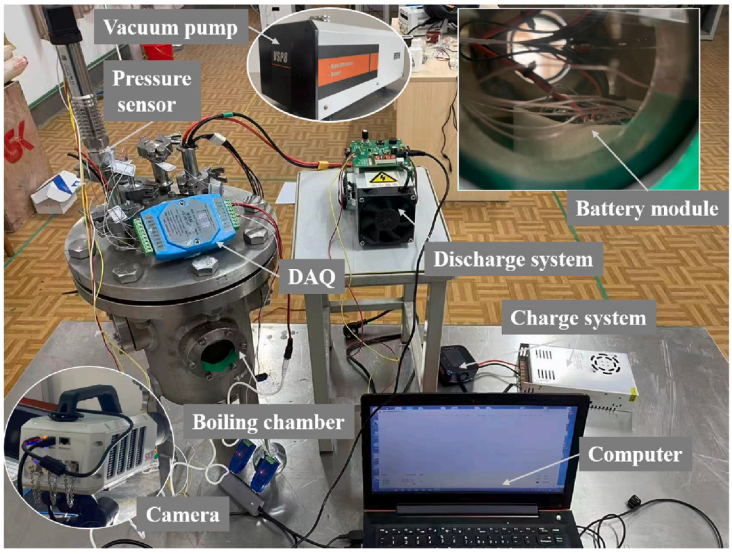

(b) Photograph of pool boiling battery module cooling system

Fig.4. Pool boiling battery module cooling system.

module operated at discharge rates ranging from 1.0 C to 2.5 C. During the experiments, parameters including battery temperature, current, voltage, and system pressure were continuously recorded using a data acquisition system. Each operating condition was repeated three times to verify the reproducibility of the experimental results.

2.3. Data processing

Under near-adiabatic conditions, the heat generated by the battery during discharge is mainly converted into the temperature rise of the battery itself, while heat exchange with the surrounding environment can be neglected. According to the principle of energy conservation, the instantaneous heat generation rate during discharge can be estimated from the rate of temperature change, which can be expressed as:

$$Q_{gen} = mc_p \frac{dT}{dt} \tag{1}$$

where Q_{gen} denotes the instantaneous heat generation rate of the battery, m is the battery mass, c_p is the effective specific heat capacity of the battery, and dT/dt is the temperature rise rate. This method has been widely adopted in battery thermal characterisation under near-adiabatic conditions, where the heat generated by the battery is assumed to be primarily stored within the cell due to the negligible heat loss to the surroundings during the short discharge period. Therefore, the heat generation rate can be estimated directly from the measured battery temperature rise.

At each time instant t, the temperatures measured at the twenty-one locations on the battery module are denoted as $T_i(t)(i = 1, \cdots, 21)$. The instantaneous maximum temperature is defined as:

$$T_{\max}(t) = \max\{T_1(t), T_2(t), \cdots, T_{21}(t)\} \tag{2}$$

while the instantaneous temperature non-uniformity is defined as:

$$\Delta T(t) = \max\{T_1(t), \cdots, T_8(t)\} - \min\{T_1(t), \cdots, T_{21}(t)\} \tag{3}$$

The maximum battery temperature during a discharge process is determined as:

$$T_{\max} = \max_{t\in[t_0,t_{\text{end}}]} T_{\max}(t) \tag{4}$$

The maximum temperature difference during discharge is defined as:

$$\Delta T^{\text{dis}} = \max_{t\in[t_0,t_{\text{end}}]} \Delta T(t) \tag{5}$$

The auxiliary energy consumption required for pressure regulation was directly measured using an electricity meter during each discharge experiment. Therefore, the auxiliary energy consumption was not estimated from the rated power of the vacuum pump. For each pressure condition, the cumulative electrical energy consumption of the pressure regulation system was recorded over the entire discharge period. The average auxiliary power was then calculated as:

$$P_{\text{aux}} = \frac{E_{\text{aux}}}{t_{\text{dis}}} \tag{6}$$

where P_{aux} is the average auxiliary power, E_{aux} is the measured electrical energy consumption of the pressure regulation system during the discharge test, and t_{dis} is the total discharge duration.

To evaluate the system-level trade-off between thermal performance enhancement and the associated energy cost, a cooling efficiency metric is defined as:

$$\eta_T = \frac{T_{\max,\text{ref}} - T_{\max,\text{vac}}}{\bar{P}_{\text{vac}}} \tag{7}$$

where $T_{\max,\text{ref}}$ and $T_{\max,\text{vac}}$ denote the maximum battery surface temperatures under the reference pressure condition and sub-atmospheric pressure condition, respectively.

2.4. Uncertainty analysis

The measurement uncertainty in this study mainly arises from the temperature sensors, pressure sensor, electrical measurement devices, battery test system, and data acquisition system. Calibrated K-type thermocouples were used for battery surface temperature measurements, with a manufacturer-specified accuracy of ±0.5 °C within the operating temperature range. The pressure inside the boiling chamber was monitored using a calibrated pressure transducer with an accuracy of ±0.5 kPa. Electrical current and voltage were measured using a battery test system with accuracies better than ±0.5 %, ensuring reliable determination of the operating conditions during charge and discharge.

For a calculated variable $Y = f(x_1, x_2, \cdots, x_n)$, the combined standard uncertainty was evaluated using the root-sum-square method based on the propagation of uncertainties [37]:

$$u_Y = \sqrt{\sum_{i=1}^{n} \left(\frac{\partial Y}{\partial x_i} u_{x_i}\right)^2} \tag{8}$$

where u_Y is the combined standard uncertainty of Y, u_{x_i} is the standard uncertainty of the measured variable x_i, and $\partial Y/\partial x_i$ is the sensitivity coefficient of Y with respect to x_i.

The heat generation rate of the battery was calculated from the near-adiabatic temperature rise experiment. Its uncertainty was evaluated by considering the uncertainties of battery mass, equivalent specific heat capacity, temperature measurement, and temperature rise rate. The expanded relative uncertainty of the calculated heat generation rate was estimated to be within ±7.1%.The measurement uncertainties of the main experimental parameters and instruments are summarised in Table 4.

3. Thermo–lifetime–economic coupling model

3.1. Modelling assumptions

The proposed thermo–lifetime–economic model is established based on a set of simplifying assumptions:

(1) An Arrhenius-type relation is adopted to describe temperature-dependent ageing, with parameters selected from commonly reported ranges in the literature.
(2) The maximum temperature $T_{\max}$ is used to represent the dominant thermal ageing effect.
(3) The maximum temperature difference $\Delta T_{\max}$ is used to characterise temperature non-uniformity within the battery module.
(4) The temperature difference penalty coefficient λ is treated as an empirical parameter.
(5) In the economic model, battery cost scales linearly with system size, while auxiliary energy consumption is assumed independent of scale within a certain range.

Therefore, the model outputs should be interpreted as relative indicators, representing the comparative trends in thermal performance, lifetime, and economic cost under different operating conditions.

3.2. Temperature-induced lifetime model

Battery degradation is strongly influenced by temperature, as many ageing mechanisms are governed by thermally activated processes and can be approximately described by Arrhenius-type behaviour [38,39]. In this study, a simplified temperature-based lifetime metric is introduced to evaluate the relative influence of different pressure conditions. It should be noted that this model provides an approximate comparison rather than an accurate prediction of absolute battery lifetime. The maximum battery temperature under the 2.5C condition at 100 kPa is selected as the reference temperature. Based on this, a relative lifetime factor is defined as:

$$AF_i = \exp\left[\frac{E_a}{R}\left(\frac{1}{T_i} - \frac{1}{T_{ref}}\right)\right] \tag{9}$$

where AF_i denotes the relative lifetime factor; E_a is the apparent activation energy; R is the universal gas constant; T_i is the characteristic temperature and T_{ref} is the reference temperature.

3.3. Temperature uniformity correction model

In addition to the maximum battery temperature, temperature non-uniformity also has a significant impact on battery lifetime [40]. A large temperature difference leads to inconsistent degradation rates among batteries. This further accelerates overall performance

Table 4
Measurement uncertainty of the experimental system.

Parameter	Instrument	Uncertainty
Battery surface temperature	K-type thermocouple	±0.5 °C
Chamber pressure	Pressure transducer	±0.5 kPa
Voltage	Battery test system	±0.5 %
Current	Battery test system	±0.5 %
Time	Data acquisition system	±0.1 s
Heat generation rate	Uncertainty propagation	±7.1 %
Pressure fluctuation during operation	Pressure control system	±0.8 kPa
Auxiliary energy consumption	Electricity meter	±0.5%

degradation. A temperature difference correction term is therefore introduced. A corrected lifetime index is then defined as:

$$BI_i = \exp\left[\frac{E_a}{R}\left(\frac{1}{T_i} - \frac{1}{T_{ref}}\right)\right] \cdot \frac{1 + \beta\Delta T_{ref}}{1 + \beta\Delta T_i} \tag{10}$$

where LBI_i denotes the integrated lifetime benefit index; ΔT_i is the maximum temperature difference under the i-th operating condition; ΔT_{ref} is the reference temperature difference and β is the temperature difference penalty coefficient, taken as 0.04 [41].

3.4. Equivalent lifetime model

The cycle life under the reference condition is assumed to be L_{ref}. The equivalent lifetime under different operating conditions can then be expressed as:

$$L_i = LBI_i \cdot L_{ref} \tag{11}$$

It should be noted that no long-term ageing tests were conducted in this study. Therefore, the lifetime analysis is used as a relative evaluation tool to assess the influence of different cooling conditions on battery ageing behaviour, rather than to predict the absolute service lifetime of the battery.

To evaluate the influence of parameter uncertainty on the lifetime assessment, a sensitivity analysis was conducted by varying the temperature-difference penalty coefficient (β) by ±20% from its baseline value of 0.04. This coefficient is an empirical parameter adopted from the literature and may vary depending on battery type and operating conditions.

3.5. Lifetime-informed economic model

The economic performance is closely related to battery degradation and system energy consumption. In this study, a lifetime-based economic assessment model is developed to evaluate the relative performance of pool boiling and pressure-controlled pool boiling under different pressure conditions. It should be noted that this model is based on simplified assumptions and is intended for trend analysis rather than an accurate prediction of actual economic performance. The unit lifetime cost is introduced as a metric for economic performance under different operating conditions. It is defined as:

$$C_{\mathrm{life}} = \frac{C_{\mathrm{battery}}}{L_{\mathrm{eq}}} \tag{12}$$

where C_{battery} is the battery cost, and L_{eq} is the equivalent lifetime obtained from the proposed lifetime model. This metric reflects the cost per effective service life of the battery.

In addition to lifetime-related cost, the auxiliary energy consumption of the cooling system is considered. The auxiliary energy consumption was directly measured using an electricity meter during operation under different pressure conditions and was subsequently used for the economic analysis. The corresponding auxiliary energy cost is expressed as:

$$C_{\mathrm{energy}} = E_{\mathrm{aux}} c_{\mathrm{e}} \tag{13}$$

where C_{energy} is the auxiliary energy cost, E_{aux} is measured auxiliary electrical energy consumption during the discharge experiment, and c_{e} is the electricity price.

For pressure-controlled pool boiling, the additional energy consumption associated with pressure regulation is included in P_{aux}. This mainly arises from the operation of vacuum pumps or pressure control devices. Therefore, compared with conventional pool boiling, pressure-controlled systems generally exhibit higher operational costs.

The total economic cost of a pressure-regulated pool boiling cooling system can be expressed as:

$$C_{\mathrm{total}} = C_{\mathrm{lifetime}} + C_{\mathrm{energy}} + C_{\mathrm{capital}} + C_{\mathrm{maintenance}} \tag{14}$$

where C_{lifetime}, C_{energy}, C_{capital}, and $C_{\mathrm{maintenance}}$ represent the lifetime-related cost, auxiliary energy cost, capital cost, and maintenance cost, respectively.

In the present study, only C_{lifetime} and C_{energy} were quantitatively evaluated, because they can be directly determined from the measured thermal performance, relative lifetime index, and auxiliary energy consumption. The capital and maintenance costs of the pressure-control system were not included in the quantitative analysis, as the current setup was designed for laboratory-scale experiments rather than cost-optimised engineering deployment.

3.6. System-scale economic model

The economic analysis above is conducted at the experimental module scale. However, battery thermal management systems typically operate at much larger energy capacities [42]. It is therefore necessary to evaluate the influence of system scale on economic performance. A system scale factor s is introduced, defined as the ratio of the actual system energy capacity to that of the experimental module. The battery cost is assumed to scale linearly with system size, while the auxiliary energy consumption is assumed to remain approximately independent of system scale within a certain range. The total cost can be expressed as:

$$C_i(s) = \frac{s\, C_{\mathrm{battery}}}{L_i} + C_{\mathrm{op},i} \tag{15}$$

where the first term $\frac{s\, C_{\mathrm{battery}}}{L_i}$ represents the lifetime-related cost. It increases linearly with system scale. The second term $C_{\mathrm{op},i}$ represents the operational cost. In this study, it is assumed to be independent of system scale. The normalised total cost under different pressure conditions is analysed as:

$$Normalisedtotalcost = \frac{C_i(s)}{C_{100}(s)} \tag{16}$$

4. Results and discussion

Fig. 5 shows the variation of the battery heat generation rate with depth of discharge (DoD) at different discharge rates. The heat generation rate is initially high and gradually decreases as the discharge progresses. A slight increase appears in the later stage, which is mainly attributed to the increase in internal resistance and the intensified polarisation at high DoD. Meanwhile, the battery heat generation rate increases significantly with increasing discharge rate, mainly because

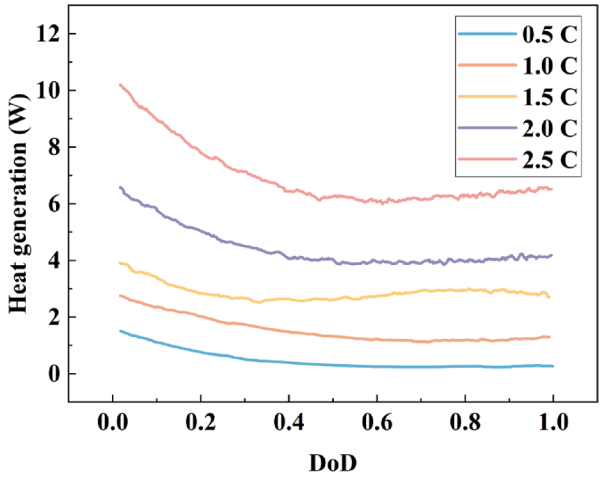

Fig.5. Heat generation rate versus DoD at different discharge rates.

the larger discharge current enhances ohmic heat generation and intensifies internal polarisation. At discharge rates of 0.5 C, 1.0 C, 1.5 C, 2.0 C, and 2.5 C, the average heat generation rates of the battery are approximately 0.6 W, 1.5 W, 2.9 W, 4.3 W, and 6.8 W, respectively. This result indicates that under high discharge rates, both ohmic heat and polarisation heat within the battery increase significantly, leading to a higher overall heat generation level. Therefore, effective control of the heat generated by the battery under high-rate conditions is crucial for maintaining temperature stability and ensuring system safety.

Fig. 6 compares the maximum temperature and maximum temperature difference of the battery module over time under different discharge rates for natural cooling and pool boiling cooling. Under natural air-cooling conditions, the maximum temperature of the battery module increases markedly with increasing discharge rate. At a discharge rate of 2.5 C, the maximum temperature of the battery module reached 88.8 °C at the end of discharge, with a corresponding maximum temperature difference of 9.3 °C. This indicates that natural air cooling is insufficient to dissipate the large amount of heat generated under high-rate discharge conditions. In natural cooling, the battery module mainly relies on heat conduction within the module and natural convection between the battery surface and the surrounding air for heat dissipation. Owing to the relatively low heat transfer coefficient of natural convection, the continuously generated heat cannot be removed in a timely manner, leading to progressive heat accumulation and a rapid increase in battery temperature [43]. In addition, the weak intensity of natural convection and the non-uniform cooling environment around different battery locations limit heat redistribution within the module. As a result, local heat accumulation is more likely to occur, causing the maximum temperature difference to increase gradually throughout the discharge process. By contrast, pool boiling cooling exhibits a pronounced temperature suppression effect at the same discharge rate. At 2.5 C, the maximum temperature at the end of discharge was reduced to 45.6 °C, representing a decrease of 46.2 °C compared with natural cooling, corresponding to a reduction of 48.6%. In addition, the maximum temperature difference under pool boiling cooling was only 3.1 °C at 2.5 C, corresponding to a reduction of 6.2 °C compared with natural cooling, which represents a decrease of 66.7%. The superior thermal performance of pool boiling cooling can be attributed to the pool boiling heat transfer mechanism. During pool boiling, bubble nucleation, growth, and departure occur on the heated battery surface [44]. This process removes a large amount of heat through latent heat absorption and disturbs the thermal boundary layer near the battery surface, promoting liquid replenishment and local convective mixing. Consequently, both the absolute temperature rise and the temperature non-uniformity of the battery module are effectively suppressed.

As shown in Fig. 7, the saturation temperature of the coolant varies significantly with system pressure. The saturation temperature increases with increasing pressure, while reducing the pressure from 100 kPa to 20 kPa decreases the saturation temperature from 64.8 °C to 27.4 °C. This indicates that pressure regulation can effectively modify the phase-change temperature of the coolant. The pressure-dependent variation in saturation temperature directly affects the wall superheat during pool boiling. For a given battery surface temperature, reducing the system pressure lowers the coolant saturation temperature, thereby increasing the effective wall superheat. A higher wall superheat provides a stronger thermodynamic driving force for bubble nucleation and promotes an earlier transition from natural convection or weak nucleate boiling to more active nucleate boiling. Previous studies have shown that this transition plays an important role in improving boiling heat transfer efficiency [23,45]. A commonly recommended operating temperature

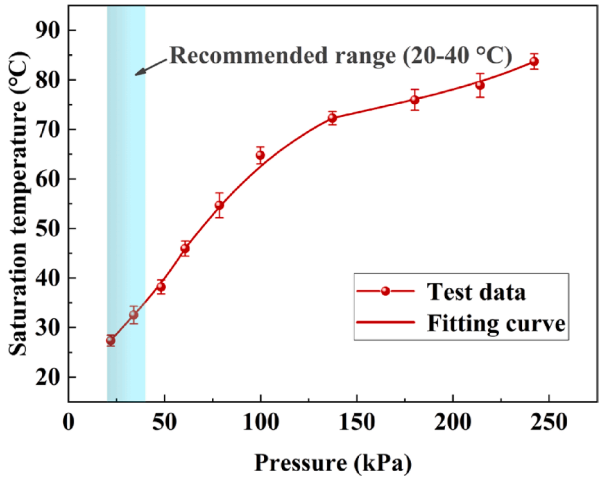

Fig.7. Variation of the coolant saturation temperature with system pressure.

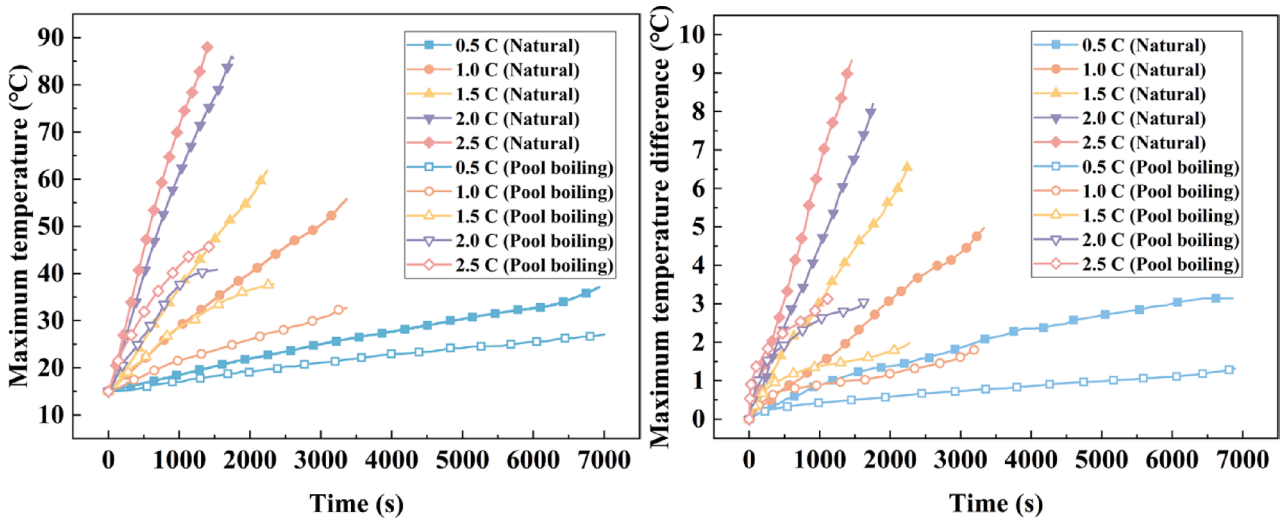

Fig.6. Thermal behaviour of the battery module for natural and pool boiling cooling.

range for lithium-ion batteries, 20-40 °C, is also indicated in the figure [46]. Within the pressure range of 20–50 kPa, the coolant saturation temperature falls within the recommended operating temperature range for lithium-ion batteries. This suggests that low-pressure operation enables pool boiling to occur at relatively low battery surface temperatures, allowing pool boiling heat transfer to participate earlier in the cooling process. Therefore, the effectiveness of pressure regulation depends strongly on the pressure–saturation temperature characteristics of the working fluid, and different dielectric coolants may have different optimal pressure ranges.

Fig. 8(a) illustrates the temporal evolution of the maximum temperature of the battery module during 2.5 C discharge under different system pressures. During discharge, the maximum temperature increases continuously, but the temperature rise is significantly affected by system pressure. At 100 kPa, the maximum temperature increases most rapidly and reaches 45.6 °C at the end of discharge. As the pressure decreases to 70 kPa and 50 kPa, the final maximum temperatures decrease to 39.5 °C and 37.1 °C, respectively. When the pressure is further reduced to 20 kPa, the maximum temperature decreases to 33.6 °C and remains within the recommended operating temperature range for lithium-ion batteries. These results indicate that reducing system pressure significantly enhances the temperature suppression capability of pool boiling cooling for the battery module. This improvement is mainly attributed to the pressure-dependent saturation temperature of the coolant. A lower pressure reduces the coolant saturation temperature and increases the effective wall superheat, thereby strengthening the thermodynamic driving force for bubble nucleation and promoting the earlier onset of nucleate boiling [44]. Fig. 8(b) further presents the variation in the temperature rise rate of the maximum temperature under different pressures. At 100 kPa, the initial temperature rise rate is the highest, indicating that the heat removal capability remains limited before boiling-enhanced heat transfer is fully established. As discharge proceeds, the temperature rise rate decreases markedly, suggesting a gradual transition to boiling-enhanced heat transfer. Under lower-pressure conditions, this decrease occurs earlier, indicating that nucleate boiling is activated sooner. Therefore, pool boiling heat transfer can participate in heat removal from an earlier stage of discharge, effectively suppressing the sustained rapid increase in battery temperature.

The variation in the maximum temperature difference of the battery module under different system pressures is shown in Fig. 9. Under all pressure conditions, the maximum temperature difference increases progressively with discharge time, but its growth rate is clearly affected by system pressure. At 100 kPa, the maximum temperature difference increases most rapidly and remains the highest throughout the discharge process, reaching approximately 3.1 °C at the end of discharge. This is mainly because the coolant saturation temperature is relatively high at 100 kPa, and effective nucleate boiling is not fully established during the initial stage of discharge. Before boiling-enhanced heat transfer becomes fully effective, heat removal mainly relies on single-phase convection and heat conduction within the module. Therefore, local heat accumulation is more likely to occur, leading to a rapid increase in the maximum temperature difference. The maximum temperature difference continues to increase during discharge, but its growth becomes progressively slower. This indicates that the battery surface temperature gradually reaches the condition required for pool boiling, and boiling heat transfer begins to participate more effectively in heat removal. For local regions with higher temperatures, the wall superheat is larger, making bubble nucleation easier to activate and leading to more frequent bubble

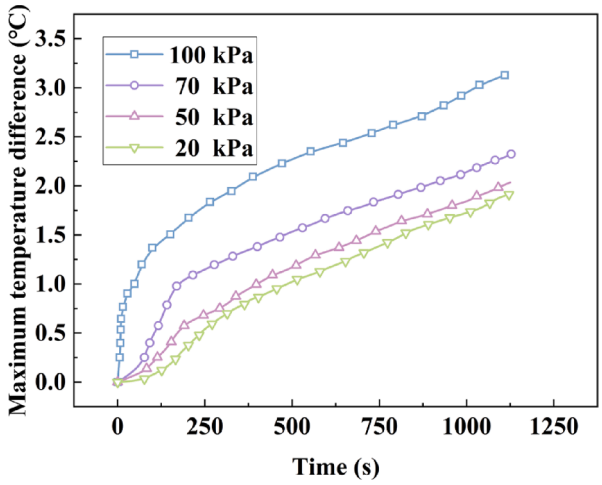

Fig. 9. Effect of system pressure on the maximum temperature difference.

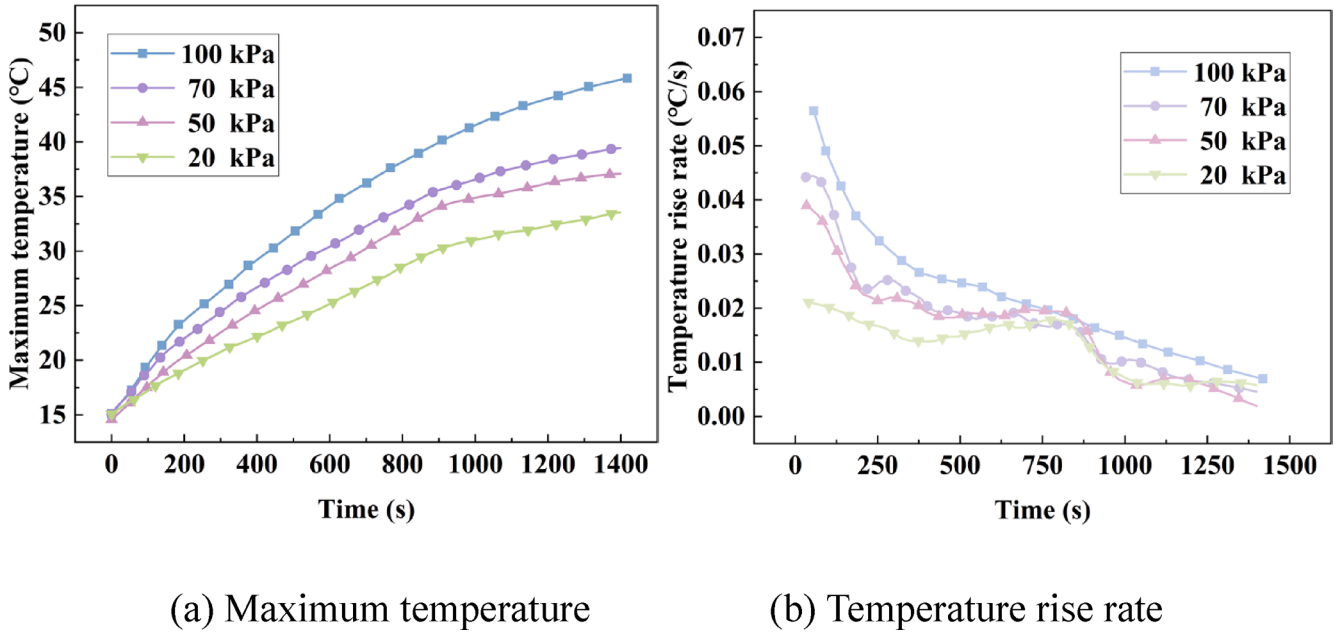

Fig. 8. Thermal behaviour of the battery module under different system pressures.

growth and departure. The intensified bubble activity disturbs the thermal boundary layer near the heated surface and promotes liquid replenishment and local convective mixing, thereby improving the local heat transfer efficiency in hotter regions [47]. Consequently, local hot spots can be cooled more rapidly, and the further development of temperature non-uniformity is suppressed. As the system pressure decreases, the maximum temperature difference of the battery module is significantly reduced. At pressures of 70 kPa, 50 kPa, and 20 kPa, the maximum temperature difference at the end of discharge decreases to approximately 2.3 °C, 2.0 °C, and 1.9 °C, respectively. This improvement can be attributed to the earlier involvement of boiling heat transfer under reduced-pressure conditions, which strengthens local heat removal in hotter regions and suppresses local hot-spot formation. As a result, the temperature uniformity of the battery module is improved [44].

Fig. 10 compares the maximum temperature and maximum temperature difference of the battery module at the end of discharge under different system pressures. When the system pressure is reduced from 100 kPa to 70 kPa, the maximum temperature decreases from 45.6 °C to 39.5 °C, corresponding to a reduction of approximately 13.8%. Further decreasing the pressure to 50 kPa lowers the maximum temperature to 37.1 °C, representing a reduction of about 19.0%. When the pressure is reduced to 20 kPa, the maximum temperature further decreases to 33.6 °C, giving an overall reduction of approximately 26.3%. The maximum temperature difference also exhibits a clear dependence on system pressure. It decreases from approximately 3.1 °C at 100 kPa to about 2.3 °C at 70 kPa, corresponding to a reduction of 25.8%. Further reductions to approximately 2.0 °C and 1.9 °C are obtained at 50 kPa and 20 kPa, respectively, giving an overall decrease of approximately 38.7%. These results indicate that, within the pressure range of 20–100 kPa, reducing system pressure can simultaneously suppress the peak temperature and improve the temperature uniformity of the battery module. However, the improvements in maximum temperature and maximum temperature difference do not increase linearly with decreasing pressure. This trend is particularly evident in the low-pressure range, where the further reduction in maximum temperature difference becomes less pronounced. This suggests that the enhancement of pool boiling heat transfer may exhibit diminishing marginal benefits under lower-pressure conditions. Therefore, the pressure-regulated cooling strategy should not be evaluated solely based on the lowest achievable battery temperature, but should also consider the balance among thermal performance improvement, boiling behaviour, and the additional energy consumption required for pressure regulation.

To further explain the non-linear thermal response observed in Fig. 10, Fig. 11 compares the boiling behaviour at the end of 2.5 C discharge, when the battery module reached its maximum temperature. The four images reveal a clear transition in the near-surface boiling behaviour as the system pressure decreases. Under 100 kPa, no distinct bubble generation can be identified near the battery surface. The weak streak-like structures are mainly associated with thermal plumes induced by natural convection and refractive-index variations caused by local temperature gradients, indicating that boiling heat transfer is not clearly activated. When the pressure is reduced to 70 kPa, isolated fine bubbles start to appear near the heated surface, suggesting the onset of weak nucleate boiling. A further decrease to 50 kPa leads to a much denser distribution of small bubbles, together with stronger liquid disturbance around the battery surface. This indicates that bubble nucleation and departure become more active, which enhances liquid renewal and local boiling heat transfer. The most intensive bubble activity is observed at 20 kPa, where fine bubbles are densely distributed near the heated surface. Although this stronger boiling activity contributes to heat removal, excessive bubble accumulation and local bubble interaction may restrict liquid replenishment and reduce the effective liquid–surface contact area. This provides a visual explanation for the diminishing improvement in maximum temperature and maximum temperature difference observed in Fig. 10 when the pressure is further reduced.

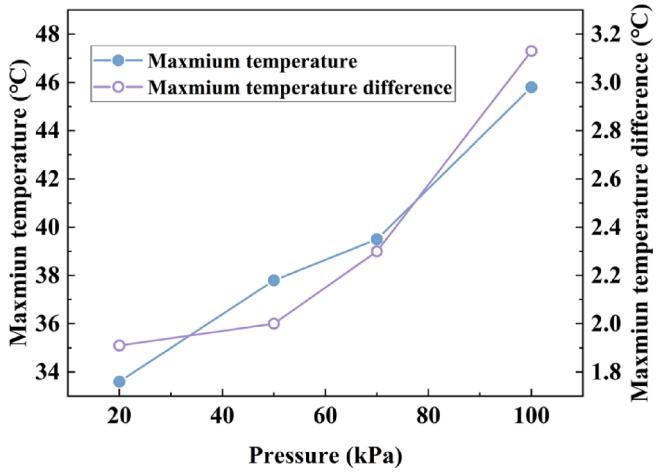

Fig. 10. Maximum temperature and temperature difference at different pressures.

Fig. 12 presents the coupled thermo-lifetime-economic behaviour of the battery module under different pressure conditions. As shown in Fig. 12(a), the auxiliary power increases significantly with decreasing pressure. When the pressure is reduced from 100 kPa to 70 kPa, the auxiliary power increases from approximately 30.0 W to 108.8 W, corresponding to an increase of about 262.7 %. A further reduction to 50 kPa increases the power to approximately 172.0 W, representing an increase of about 473.3 % relative to 100 kPa. When the pressure is decreased to 20 kPa, the auxiliary power rises sharply to approximately 467.8 W, which is increased by approximately 14.6 times relative to 100 kPa. This indicates a strong sensitivity of energy consumption to pressure reduction, particularly in the low-pressure regime. Fig. 12(b) shows the variation of the normalised lifetime. Compared with the baseline at 100 kPa, the lifetime increases to approximately 1.3, 1.4, and 1.7 times at 70, 50, and 20 kPa, corresponding to improvements of about 29.3 %, 43.4 %, and 65.1 %, respectively. This trend is consistent with the reduction in maximum temperature and temperature difference observed in Fig. 10. Fig. 12(c) shows the variation of cost composition and total cost. The lifetime-related cost decreases from 0.0111 £/cycle at 100 kPa to 0.0086, 0.0077, and 0.0067 £/cycle at 70, 50, and 20 kPa, corresponding to reductions of approximately 22.7 %, 30.3 %, and 39.5 %, respectively. In contrast, the operational cost increases from 0.0030 £/cycle at 100 kPa to 0.0107, 0.0170, and 0.0462 £/cycle, representing increases of about 262.7 %, 473.3 %, and 1460.8 %, respectively. As a result, the total cost increases from 0.0141 £/cycle at 100 kPa to 0.0193, 0.0247, and 0.0529 £/cycle at 70, 50, and 20 kPa, corresponding to increases of approximately 37.4 %, 75.8 %, and 276.5 %, respectively. The contribution of operational cost increases from about 21.1% at 100 kPa to approximately 55.6 %, 68.7 %, and 87.3 % at 70, 50, and 20 kPa, respectively. This demonstrates a clear transition in the dominant cost component. Overall, although reducing the system pressure effectively improves thermal performance and extends battery lifetime, the associated energy consumption increases disproportionately. In particular, the lifetime improvement increases by up to 65.1 %, whereas the operational energy cost increases by more than 14.6 times. This strong asymmetry indicates diminishing economic returns with further pressure reduction, especially in the low-pressure regime. The underlying thermo–lifetime–economic coupling mechanism is illustrated in Fig. 12 (d).

Fig. 13 shows the effect of system scale on the normalised total cost under different pressure conditions. At small system scales, all pressure-controlled conditions exhibit higher costs than the 100 kPa baseline. For example, at $s = 1$, the relative cost is approximately 1.4, 1.8, and 3.8 for 70, 50, and 20 kPa, respectively. This indicates that the operational

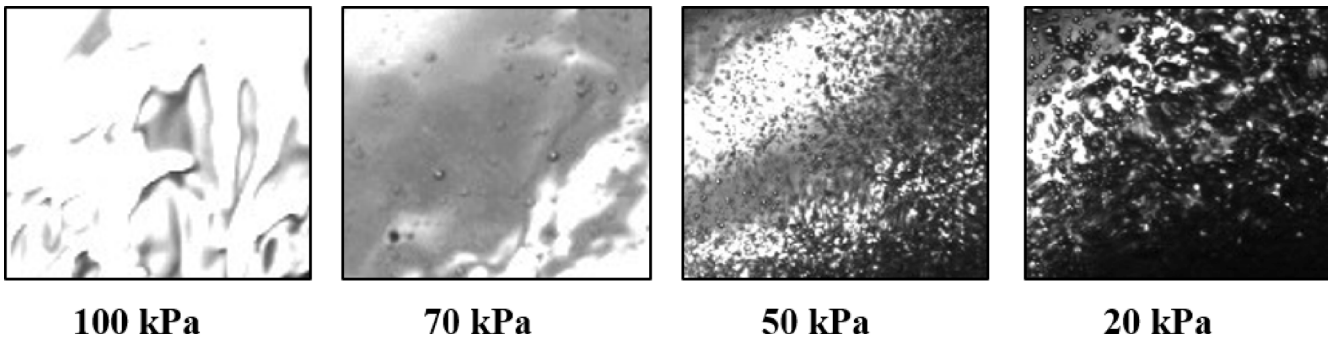

Fig.11. Visual observation of boiling behaviour under different system pressures.

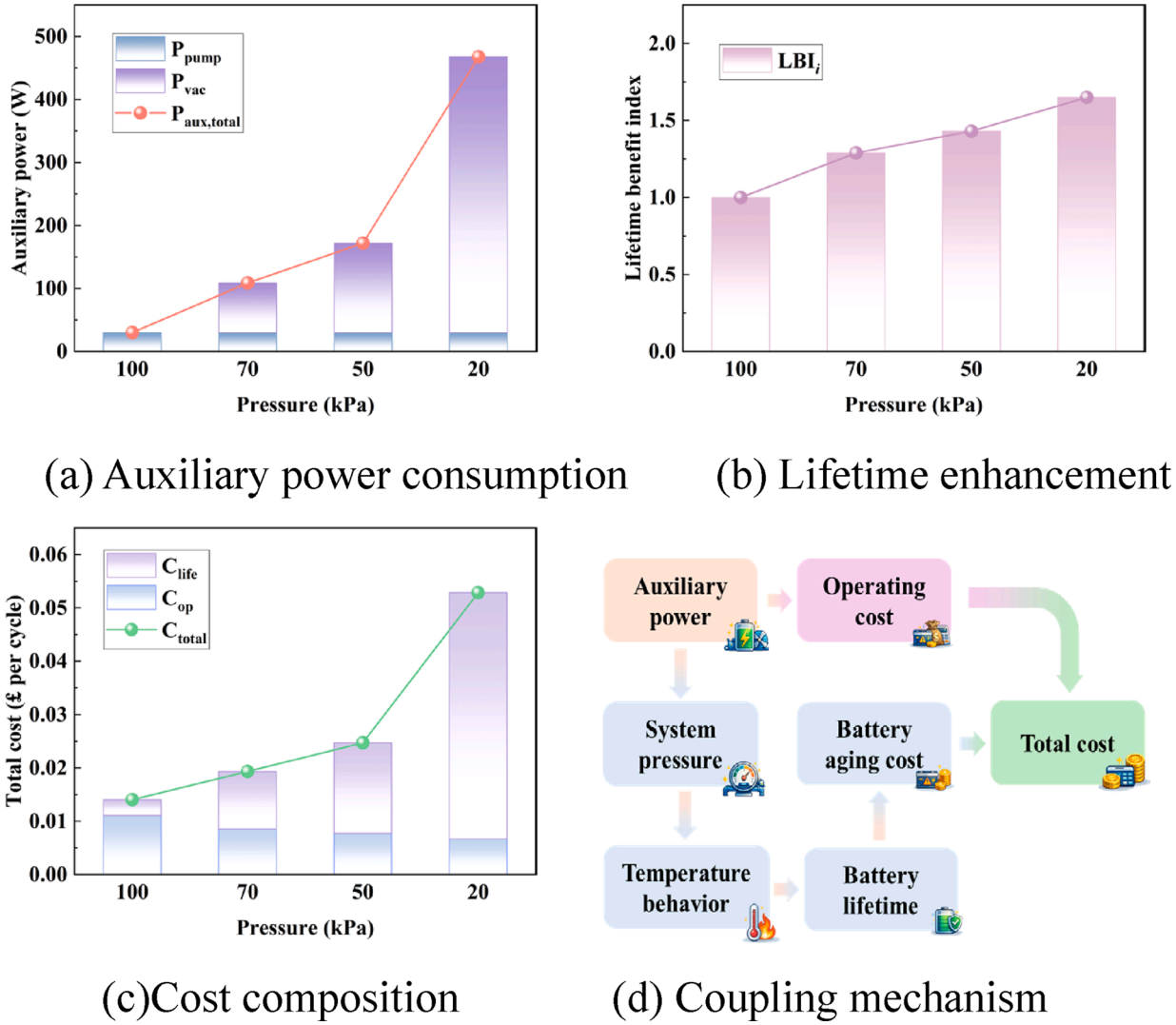

Fig. 12. Thermo–lifetime–economic performance under different pressures.

energy penalty dominates the economic performance at the experimental-module scale. As the system scale increases, the relative cost of pressure-controlled conditions decreases continuously. At $s = 2$, the cost reduces to approximately 1.1, 1.3, and 2.4 for 70, 50, and 20 kPa, respectively. This trend is attributed to the increasing contribution of lifetime-related cost, which scales with system size, while the operational cost remains approximately constant. The critical scale can be identified from the intersection with the baseline cost. The 70 kPa condition reaches this threshold at approximately $s = 3.1$, followed by the 50 kPa condition at $s = 4.2$. In contrast, the 20 kPa condition requires a much larger scale, reaching the threshold at approximately $s = 9.9$. Beyond the critical scale, pressure-controlled operation becomes economically favourable. For instance, at $s = 5$, the relative cost decreases to approximately 0.9 and 1.0 for 70 and 50 kPa, respectively, while at $s = 10$, all pressure-controlled conditions approach or fall below the baseline cost. These results demonstrate that the economic feasibility of pressure-controlled pool boiling is strongly scale-dependent. Moderate pressure reduction (70 kPa) becomes

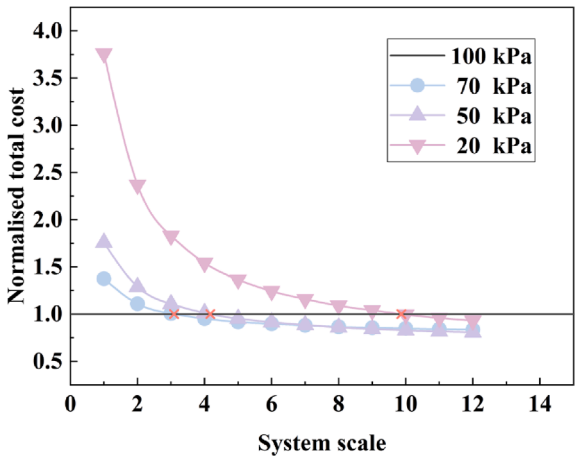

Fig. 13. Thermo–economic scaling behaviour under different pressures.

economically attractive at relatively small system scales, whereas deeper pressure reduction requires significantly larger systems to offset the associated energy penalty.

Table 5 presents the sensitivity analysis results obtained by varying the temperature-difference penalty coefficient (β) by ± 20%. Although the absolute value of the lifetime benefit index changes slightly with β, the relative ranking of different pressure conditions remains unchanged. The 20 kPa condition consistently exhibits the highest lifetime benefit, followed by 50 kPa, 70 kPa, and 100 kPa. The maximum deviation from the baseline result is less than 1%, indicating that the proposed thermo–lifetime–economic conclusions are robust with respect to reasonable variations in the model parameter.

5. Limitations and Future Work

Although the effectiveness of the pressure-regulated pool boiling cooling strategy has been demonstrated in this study, its large-scale implementation and practical deployment still require further consideration regarding coolant sustainability, material compatibility, and long-term operational reliability.

First, coolant sustainability and environmental impact remain important issues for practical immersion cooling applications. Although KEY-116 exhibits favourable heat transfer and dielectric insulation characteristics, the selection of dielectric coolants should consider not only thermal management performance but also safety, environmental impact, long-term stability, and regulatory constraints. Recent reviews on immersion cooling for data centres, electric vehicles, battery thermal management, and electronic components have highlighted that dielectric-fluid selection should account for thermal performance, electrical insulation, non-flammability, environmental impact, and long-term deployment challenges [48–51]. Therefore, the development and evaluation of dielectric coolants with lower environmental impacts remain important directions for future research.

Second, material compatibility is another critical factor for the practical implementation of immersion battery cooling systems. Battery packs contain various metals, polymers, elastomers, sealing materials, and adhesive components, and their long-term interaction with dielectric coolants may affect system reliability. Recent reviews on Li-ion battery immersion cooling have emphasised that coolant compatibility with battery-pack materials and auxiliary components should be carefully evaluated before large-scale deployment [50,51]. In the present experiments, no obvious material degradation, leakage, swelling, or operational abnormality was observed for the KEY-116 coolant, the test system, or the battery module during the experimental period. Nevertheless, the present study did not include long-term compatibility or durability testing. Therefore, future work should include long-term coolant stability assessment, material compatibility testing, and validation under repeated thermal cycling and practical operating environments.

Table 5
Sensitivity analysis of β.

Pressure (kPa)	β = 0.032 (−20%)	β = 0.040 (Baseline)	β = 0.048 (+20%)
100	1.000	1.000	1.000
70	1.182	1.186	1.190
50	1.341	1.349	1.356
20	1.638	1.651	1.664

6. Conclusion

This study presents a systematic experimental investigation of pressure-controlled pool boiling cooling for lithium-ion battery modules and establishes a coupled thermo–lifetime–economic evaluation framework. The main conclusions are summarised as follows:

(1) Pool boiling cooling significantly enhances the thermal performance of the battery module compared with natural cooling. At 2.5 C, the maximum temperature is reduced by 48.6%, while the maximum temperature difference is decreased by 66.7%, demonstrating the superior capability of pool boiling heat transfer in suppressing temperature rise and improving thermal uniformity.

(2) System pressure plays a dominant role in governing the boiling behaviour by regulating the saturation temperature and wall superheat. Reducing pressure promotes an earlier onset of nucleate boiling, thereby enhancing heat transfer. As the pressure decreases from 100 kPa to 20 kPa, the maximum temperature and temperature difference are reduced by 26.3% and 38.7%, respectively.

(3) The thermal enhancement exhibits a clear diminishing return with further pressure reduction. For instance, the reduction in maximum temperature difference decreases from 25.8% (100–70 kPa) to 13.0% (70–50 kPa), and further to only 5.0% (50–20 kPa), indicating progressively smaller thermal gains in the low-pressure regime.

(4) A strong thermo-economic trade-off is identified. While reducing pressure improves battery lifetime by up to 65.1%, the auxiliary energy consumption increases disproportionately by more than 14.6 times. This asymmetry reveals that excessive pressure reduction results in rapidly increasing operating costs while providing limited additional thermal benefits.

(5) The economic feasibility of pressure-controlled pool boiling cooling is strongly dependent on system scale. Moderate pressure reduction becomes economically favourable at relatively small scales, whereas deeper pressure reduction requires significantly larger systems to offset the additional energy consumption. These results highlight the importance of considering both thermal performance and operating costs when determining system operating conditions.

Overall, system pressure should be treated as a key operating parameter in pressure-controlled pool boiling cooling systems. Within the investigated conditions, an appropriate pressure range enables a balanced trade-off between thermal performance, battery lifetime, and operating cost. The proposed thermo–lifetime–economic coupling framework provides an effective approach for evaluating the performance of pressure-controlled pool boiling cooling under the studied operating conditions. Future work will focus on the development of dynamic pressure regulation strategies, validation under realistic vehicle operating conditions, and the establishment of more comprehensive thermo–lifetime–economic models incorporating additional operational and system-level factors.

CRediT authorship contribution statement

Xiang Wang: Writing – original draft, Visualization, Methodology, Investigation, Conceptualization. **Liang Li:** Writing – review & editing, Funding acquisition. **Savvas A. Tassou:** Supervision.

Declaration of competing interest

The authors declare that they have no known competing financial interests or personal relationships that could have appeared to influence the work reported in this paper.

Data availability

Data will be made available on request.

References

[1] Wu W, Wang S, Wu W, et al. A critical review of battery thermal performance and liquid based battery thermal management. Energy Convers. Manag. 2019;182:262–81.
[2] Kim J, Oh J, Lee H. Review on battery thermal management system for electric vehicles. Appl. Therm. Eng. 2019;149:192–212.
[3] Gharehghani A, Rabiei M, Mehranfar S, et al. Progress in battery thermal management systems technologies for electric vehicles. Renew. Sustain. Energy Rev. 2024;202:114654.
[4] Thakur AK, Sathyamurthy R, Velraj R, et al. A state-of-the-art review on advancing battery thermal management systems for fast-charging. Appl. Therm. Eng. 2023;226:120303.
[5] Jiang ZY, Li HB, Qu ZG, et al. Recent progress in lithium-ion battery thermal management for a wide range of temperature and abuse conditions. Int. J. Hydrogen Energy 2022;47:9428–59.
[6] Wu N, Chen Y, Lin B, et al. Thermal performance evaluation of boiling cooling system for the high-rate large-format lithium-ion battery under coolant starvation. J. Energy Storage 2022;55:105616.
[7] Tang Z, Ji Y, Sun R, et al. Simulation study on thermal performance of an indirect boiling cooling cylindrical battery system with two-phase coolant R141b. Energy Technol. 2023;11:2300631.
[8] Tang K, Jia M, Zhong G, et al. Pool boiling heat transfer of dual-scale porous microchannel for high-power electronics cooling. Int. Commun. Heat Mass Transf. 2022;138:106339.
[9] Wang Z, Han W, Liu J, et al. Experimental investigation on pool boiling heat transfer enhancement with a composite structure of coiled wires and cavities. Int. Commun. Heat Mass Transf. 2026;172:110557.
[10] Yao KM, Xu M, Yang S, et al. Pool boiling heat transfer characteristics of porous nickel microstructure surfaces. J. Enhanced Heat Transf. 2024;31.
[11] Chen K, Tang A, Pan J, et al. Experimental study on heat transfer characteristics and capillary-assisted enhancement of dual-phase immersion battery thermal management system. Energy Convers. Manag. 2024;322:119149.
[12] Wang Y, Li C, Wen X, et al. Experimental studies on two-phase immersion liquid cooling for Li-ion battery thermal management. J. Energy Storage 2023;72:108748.
[13] Sun Y, Tang Y, Zhang S, et al. A review on fabrication and pool boiling enhancement of three-dimensional complex structures. Renew. Sustain. Energy Rev. 2022;162:112437.
[14] Pereira J, Souza R, Lima R, et al. An overview of the recent advances in pool boiling enhancement materials, structures, and devices. Micromachines 2024;15:281.
[15] Qi W, Liu Y, Wang X, et al. Performance enhancement of battery thermal management based on liquid cooling plate channels embedded with non-uniform spiral fin structures. Appl. Therm. Eng. 2026;257:131501.
[16] Lyu P, Xiao Y, Fan X, et al. Effect of battery surface microtopography on immersion boiling thermal management for lithium-ion batteries. Renew. Energy 2025;124258.
[17] Williams NP, Trimble D, O'Shaughnessy SM. An experimental investigation of liquid immersion cooling of a four-cell lithium-ion battery module. J. Energy Storage 2024;86:111289.
[18] Kim YI, Jang K, Park C, et al. Enhanced cooling of high-power microelectronics with swing-like pool boiling. Int. Commun. Heat Mass Transf. 2021;125:105338.
[19] A.K. Il'sat, M.D. Filippov, A.V. Tupotilova, et al. Pressure effect on pool boiling heat transfer characteristics of high-volatile liquids with structured surface. Interfacial Phenom. Heat Transf. 2024;12.
[20] Kim SJ, Yong H, Yoo HS, et al. From water to dielectric fluids: Pool boiling research under pressure and subcooling for next-generation cooling. Renew. Sustain. Energy Rev. 2026;239:116852.
[21] Yu J, Chen Z, Utaka Y. Effect of liquid static pressure on critical heat flux characteristics in low-pressure pool boiling for dielectric fluid Novec 7100. Int. Commun. Heat Mass Transf. 2025;167:109243.
[22] He W, Han J, Liu Y, et al. Vapor bubble growth and model assessment in saturated pool boiling of water across a wide range of pressures. Phys. Fluids 2025;37:023387.
[23] Van Gils RW, Danilov D, Notten PHL, van den Bosch PPJ. Battery thermal management by boiling heat-transfer. Energy Convers. Manag. 2014;79:9–17.
[24] Al-Zareer M, Dincer I, Rosen MA. Novel thermal management system using boiling cooling for high-powered lithium-ion battery packs for hybrid electric vehicles. J. Power Sources 2017;363:291–303.
[25] Jithin KV, Rajesh PK. Numerical analysis of single-phase liquid immersion cooling for lithium-ion battery thermal management using different dielectric fluids. Int. J. Heat Mass Transf. 2022;188:122608.
[26] Li Y, Bai M, Zhou Z, et al. Thermal management for the 18650 lithium-ion battery pack by immersion cooling with fluorinated liquid. J. Energy Storage 2023;73:109166.
[27] Li C, Wang Y, Sun Z, et al. Two-phase immersion liquid cooling system for 4680 Li-ion battery thermal management. J. Energy Storage 2024;97:112952.
[28] Jiang X, Zhang D, Wang Y, et al. Immersed evaporation and cell inversion: Achieving optimal cooling efficiency for batteries. Energy 2025;320:135343.
[29] Wang H, Wang Z, Huang D, et al. Analysis of dynamic characteristics of single-phase/two-phase immersion cooling battery module under sloshing excitations. Int. J. Heat Mass Transf. 2025;242:126824.
[30] Sugiarto L, Huang Z, Lu YC. Battery lifetime prediction using surface temperature features from early cycle data. Energy Environ. Sci. 2025;18:2511–23.
[31] Zheng F, et al. Temperature dependent power capability estimation of lithium-ion batteries for hybrid electric vehicles. Energy 2016;113:64–75.
[32] Seo J, et al. Effects of ambient temperature on electric vehicle range considering battery performance, powertrain efficiency, and HVAC load. Energy Convers. Manag. 2025;326:119493.
[33] Min H, et al. A thermal management system control strategy for electric vehicles under low-temperature driving conditions considering battery lifetime. Appl. Therm. Eng. 2020;181:115944.
[34] Samsung SDI Co., Ltd., Specification of Product: Lithium-ion Rechargeable Cell, Model INR21700-50G, Version No. V1.0.
[35] Leng F, Tan CM, Pecht M. Effect of temperature on the aging rate of Li ion battery operating above room temperature. Sci. Rep. 2015;5:12967.
[36] Zhongkewei New Materials (Shenzhen) Co., Ltd., Technical Data Sheet of KEY-116 Electronic Coolant, Shenzhen, China, 2026.
[37] Moffat RJ. Describing the uncertainties in experimental results. Exp. Therm. Fluid Sci. 1988;1:3–17.
[38] Kucinskis G, et al. Arrhenius plots for Li-ion battery ageing as a function of temperature, C-rate, and ageing state: An experimental study. J. Power Sources 2022;549:232129.
[39] Tian J, Xiong R, Shen W. State-of-health estimation based on differential temperature for lithium ion batteries. IEEE Trans. Power Electron. 2020;35:10363–73.
[40] Yang N, et al. Unbalanced discharging and aging due to temperature differences among the cells in a lithium-ion battery pack with parallel combination. J. Power Sources 2016;306:733–41.
[41] Mama M, et al. Comprehensive review of multi-scale lithium-ion batteries modeling: From electro-chemical dynamics up to heat transfer in battery thermal management system. Energy Convers. Manag. 2025;325:119223.
[42] Hwang FS, Confrey T, Reidy C, Picovici D, Callaghan D, Culliton D, et al. Review of battery thermal management systems in electric vehicles. Renew. Sustain. Energy Rev. 2024;192:114171.
[43] Kalkan O, Celen A, Bakirci K. Experimental and numerical investigation of the LiFePO4 battery cooling by natural convection. J. Energy Storage 2021;40:102796.
[44] Wang X, Liang K, Xu J, et al. Experimental study on bubble dynamics and heat transfer of pool boiling at sub-atmospheric pressures. Int. Commun. Heat Mass Transf. 2023;148:107065.
[45] Wang X, Yang C, Xu C, Zhu H, Chen X, Liang K, et al. Correlation of pool boiling heat transfer and enhancement by microstructure surfaces at sub-atmospheric pressures. Int. J. Heat Mass Transf. 2024;226:125465.
[46] Zhou Z, Chen S, Luo M, et al. Effect of mechanical vibration on phase change material based thermal management system for a cylindrical lithium-ion battery at high ambient temperature and high discharge rate. Int. J. Heat Mass Transf. 2023;211:124255.
[47] Youssoufi S, Riaz A, Balaras E. Direct numerical simulations of subcooled pool boiling: Studies of heat transfer and bubble dynamics. Phys. Fluids 2025;37:023393.
[48] Zheng S, Su C, Yang X, et al. A comprehensive review of single-phase immersion cooling in data centres. Appl. Therm. Eng. 2025;272:126385.
[49] Wahab A, Senobar H, Amjady N, et al. Immersion cooling innovations and critical hurdles in Li-ion battery cooling for future electric vehicles. Renew. Sustain. Energy Rev. 2025;211:115268.
[50] Xin Z, Tang W, Yao W, et al. A review of thermal management of batteries with a focus on immersion cooling. Renew. Sustain. Energy Rev. 2025;217:115751.
[51] Volodin OA, Shvetsov DA, Serdyukov VS, et al. Enhanced boiling and evaporation of dielectric fluids on modified surfaces for immersion cooling of electronic components: A review. Appl. Therm. Eng. 2025;277:127088.